Fall 2021

Computational Analysis of Changing Wavelength on Bottom Rib and Side Rib Wavy Microchannel Heat Sinks

Ty C. Kieger
San Jose State University

COMPUTATIONAL ANALYSIS OF CHANGING WAVELENGTH ON BOTTOM RIB AND SIDE RIB WAVY MICROCHANNEL HEAT SINKS

A Thesis

Presented to

The Faculty of the Mechanical Engineering

San José State University

In Partial Fulfillment

of the Requirements for the Degree

Master of Science

by

Ty C. Kieger

December 2021

The Designated Thesis Committee Approves the Thesis Titled

COMPUTATIONAL ANALYSIS OF CHANGING WAVELENGTH ON BOTTOM RIB AND SIDE RIB WAVY MICROCHANNEL HEAT SINKS

by

Ty C. Kieger

APPROVED FOR THE MECHANICAL ENGINEERING

SAN JOSÉ STATE UNIVERSITY

December 2021

Farzan Kazemifar, Ph.D.	Department of Mechanical Engineering
Nicole Okamoto, Ph.D.	Department of Mechanical Engineering
John Lee, Ph.D.	Department of Mechanical Engineering

ABSTRACT

COMPUTATIONAL ANALYSIS OF CHANGING WAVELENGTH ON BOTTOM RIB AND SIDE RIB WAVY MICROCHANNEL HEAT SINKS

by Ty C. Kieger

As the power capacity of microelectronics continues to increase while their volume and size decrease, many different on-chip methods including microchannel heat sinks (MCHS) are being explored to cool down the temperature of these electronics. Wavy MCHS have been proven to yield better heat transfer performance compared to straight MCHS, while only producing a slightly larger pressure drop. This study investigates the heat transfer performance of MCHS following a vertical wavy design and a horizontal wavy design that have the same cross-sectional area. The simulations show that vortices are produced along the channel in the peaks and troughs of the sinusoidal waves which creates mixing within the coolant to better dissipate the heat via convection. The vertical wavy design produces to long symmetrical vortices that travel along the side of the channel, while the horizontal wavy design produces four smaller symmetrical vortices that form at the top, middle, and bottom of the channel. The results show that the horizontal wavy design performs better than the straight and vertical wavy channel especially with a larger decrease in wavelength along the flow direction.

Keywords – Heat Transfer, Wavy Microchannel Heat Sinks, Computational Fluid Dynamics (CFD)

TABLE OF CONTENTS

List of Tables vi

List of Figures vii

1 Introduction 1

2 Methodology 7
2.1 Model Validation 7
2.2 Model Validation – Geometry 7
2.3 Model Validation – Meshing 10
2.4 Model Validation – Simulation 11
2.5 Simulation Method 15
2.6 Geometric Design 16

3 Results and Discussion 20
3.1 Model Validation – Results 20
3.2 Simulation Results – Constant Amplitude and Constant Wavelength 24
3.3 Simulation Results – Constant Amplitude and Changing Wavelength 29

4 Summary and Conclusion 34

References 35

LIST OF TABLES

Table 1 Thermophysical Properties of the Solid and Fluid Used 7

Table 2 Geometric Parameters of Wavy MCHS Studied by Sui et al. [7].....8

Table 3 Mesh Sizes and Computational Time 10

Table 4 Mesh Quality Criteria for All Meshes 11

Table 5 Thermophysical Properties of the Solid and Fluid Used 15

Table 6 Constant Geometric Parameters of Wavy MCHS 18

Table 7 Friction Factor and Nusselt Number at Re = 300 and Re = 800 for All Inlet Cases With Coarse Mesh 24

LIST OF FIGURES

Fig. 1. Geometry of single wavy channel of 3D model from Sui et al. [7] experiments. 8

Fig. 2. Geometry of single wavy channel with extended wavy inlet. 9

Fig. 3. Geometry of single wavy channel with extended straight inlet. 9

Fig. 4. Normalized residuals vs. iterations at Re = 800 for coarse mesh. 12

Fig. 5. Boundary conditions imposed on CFD model for model validation. 14

Fig. 6. Normalized residuals vs. iterations for vertical wavy MCHS with constant amplitude and constant wavelength at Re = 500 15

Fig. 7. Boundary conditions imposed for the CFD simulations. 16

Fig. 8. One wavy unit with A = 100 μm and λ = 1000 μm. 17

Fig. 9. Seven wavy units with $\Delta\lambda = 500$ μm and ΔA = -25 μm. 18

Fig. 10. Channel profile of wavy MCHS geometries. 18

Fig. 11. x-y plane (side) view of vertical wavy MCHS with A = 100 μm and Δλ = 300 μm. 19

Fig. 12. x-z plane (top) view of horizontal wavy MCHS with A = 100 μm and Δλ = 300 μm. 19

Fig. 13. Comparison of friction factors with experimental data from Sui et al. [7] with power trendline. 21

Fig. 14. Comparison of Nusselt numbers with experimental data from Sui et al. [7] with linear trendline.. 22

Fig. 15. Velocity vectors along z-y plane of wavy MCHS at x = 5λ. 23

Fig. 16. Velocity vectors along z-y plane of wavy MCHS at x = 5.5λ. 23

Fig. 17. Velocity vectors along z-y plane of wavy MCHS at x = 6λ. 24

Fig. 18. Y-Z plane velocity streamlines at x = 5λ, 5.25λ, 5.5λ, 5.75λ, 6λ for the vertical wavy design with A = 100 μm and λ = 2000 μm at Re = 500. 25

Fig. 19. Y-Z plane velocity streamlines at 5λ, 5.25λ, 5.5λ, 5.75λ, 6λ for the horizontal wavy design with A = 100 μm and λ = 2000 μm at Re = 500. 25

Fig. 20. Temperature contour of fluid along y-z cross section at x = 5.75λ for (a) straight, (b) vertical, and (c) horizontal with A = 100 μm and λ = 2000 μm. 27

Fig. 21. Nusselt number of straight, vertical, and horizontal wave MCHS with A = 100 μm and λ = 2000 μm.....28

Fig. 22. Pressure drop across the heatsinks for straight, vertical, and horizontal wave MCHS with A = 100 μm and λ = 2000 μm. 28

Fig. 23. Maximum temperature difference along the bottom wall of straight, vertical, and horizontal wave MCHS with A = 100 μm and λ = 2000 μm. 29

Fig. 24. Thermal resistance of straight, vertical, and horizontal wave MCHS with A = 100 μm and λ = 2000 μm. 30

Fig. 25. Temperature contours of bottom wall for (a) straight and horizontal wavy MCHS with (b) $\Delta\lambda = 300$ μm, (c) $\Delta\lambda = 150$ μm, (d) $\Delta\lambda =$ -150 μm, (e) $\Delta\lambda =$ -300 μm. 30

Fig. 26. Nusselt number at Re = 500 as a function of Δλ.....32

Fig. 27. Maximum temperature difference along the bottom wall at Re = 500 as a function of Δλ.....32

Fig. 28. Thermal resistance at Re = 500 as a function of Δλ.....33

1 INTRODUCTION

1.1 Literature Review

Advancements in technology have brought forth the miniaturization of electronic devices while significantly increasing their power consumption. High-power density devices are quite attractive as they are very compact and allow for higher performance computing. Thermal management plays a crucial role in electronics by cooling them and maintain them at an adequate temperature at which the device can still operate. Heat sinks have been used to dissipate the heat from these devices by using their high surface area, which allows for more convection heat transfer to reduce the temperature. Tuckerman and Pease [1] first experimented on a microchannel heat sink (MCHS) and discovered that their compact size and high heat transfer performance could be useful for the cooling of electronic devices even at the cost of a higher pressure drop. This enhanced heat transfer performance is due to the MCHS having a high surface-to-volume ratio which is advantageous for increasing convection heat transfer, as well as the overall heat transfer coefficient being inversely proportional to the hydraulic diameter which results in a higher heat transfer coefficient for very small hydraulic diameters. A common classification for MCHS is given by Mehendale et al. [2], defining a microchannel as one with a hydraulic diameter between 1-100 μm. This classification of MCHS will be acknowledged for this project.

The cross-sectional shape of a MCHS can take many forms and can be used to reduce the pressure drop while considerably increasing the heat transfer performance. Wang et al. [3] conducted numerical simulations on microchannels with varying aspect ratios for rectangular, triangular, and trapezoidal shapes. They determined via Computational Fluid

Dynamics (CFD) simulations that the triangular channel produced the lowest pressure drop, however, at the expense of having the highest temperature distribution and thermal resistance and therefore being reported as the least performing channel. The trapezoidal channel was found to have a low-temperature distribution and thermal resistance performing nearly as well as the rectangular channel, but only at a very narrow hydraulic diameter leading towards a rectangular-like shape, so it was concluded that the rectangular shape is the best performing channel. These results agree with Gunnasegaran et al. [4] that heat transfer performance is best for rectangular, followed by trapezoidal, and then triangular. Their numerical results demonstrated that the rectangular channel performs best with a smaller hydraulic diameter.

The straight rectangular channel has been commonly used for heat sinks due to its easy manufacturability but often lacks in heat transfer performance due to the thickening of the thermal boundary layer in the flow direction and lack of mixing within the fluid. These two issues are significant because the heat transfer coefficient is inversely proportional to the thermal boundary layer thickness, which grows in the direction of flow while mixing within the flow enhances the heat transfer phenomenon.

It has been demonstrated by Metwally and Maglik [5] and Manglik et al. [6] that sinusoidal patterns in macro-channels create disruption and considerably decrease the thickness of the thermal and velocity boundary layer which enhances heat transfer performance and momentum. They also discovered that mixing in the flow is enhanced due to counter-rotating vortices found in the cross-sections of trough regions of the wavy channel. Sui et al. [7] conducted experiments to study the fluid flow and heat transfer effects for sinusoidal wavy microchannels with different amplitudes at varying Reynolds numbers.

Their results aligned with those of Manglik et al. [6] showing the rise in heat transfer performance for wavy channels compared to straight, but also at the expense of a small increase of pressure drop.

Many numerical studies have been conducted on left-right and up-down wavy MCHS throughout the last decade. Mohammed et al. [8] investigated the influence of amplitude for left-right wavy MCHS at different Reynolds numbers. It was concluded that the temperature of the MCHS decreased as the amplitude increased up until a certain non-dimensional wavy amplitude. Sui et al. [9] utilized CFD simulation to study the relative wavy amplitude of left-right wavy MCHS defined as amplitude/wavelength and determined that increasing the relative waviness (shorter wavelength along the flow direction) increases the convective heat transfer coefficient. It was suggested for a chip that has a hot spot in the center that the relative waviness in that area can be shortened (shorter wavelength in flow direction) to allow for adequate mixing and disturbance of the thermal boundary layer thickness to improve the heat transfer performance in that specific region. Patterns of Dean vortices, counter-rotating vortices caused by secondary motion, were also noted as a contributor to the heat transfer enhancement in the wavy channels.

The up-down wavy design has also been investigated for a superior alternative to the straight channel. Sakanova et al. [10], [11] studied up-down wavy microchannels with a focus on the effect of amplitude and wavelength, discovering that the lowest thermal resistance is achieved at higher amplitudes with shorter wavelengths. The heat transfer performance for left-right and up-down wavy designs has been studied and compared by Zhu et al. [12]. Their results showed that the up-down design was superior at shorter wavelengths

regardless of aspect ratio, channel height, or ratio of amplitude to wavelength, but both designs performed similarly at larger wavelengths. The up-down wavy design performs better at shorter wavelengths because it was found to have a lower pressure drop, which at a constant pumping power results in a low velocity that can lessen heat transfer enhancement.

The amplitude and wavelength have been observed as important parameters in enhancing the heat transfer performance of wavy MCHS. Lin et al. [13] investigated the effects of changing wavelength and amplitude for left-right MCHS. They compared wavy designs with increasing or decreasing amplitude and constant wavelength along the flow direction, wavy designs with increasing or decreasing wavelength and constant amplitude along the flow direction, and wavy designs with constant wavelength and amplitude to a straight channel design. It was concluded that the designs with a decreasing wavelength or increasing amplitude along the flow direction provided the lowest thermal resistance. It was also mentioned that an optimal design can be found by simultaneously varying the wavelength and amplitude and setting $\Delta\lambda$ equal to the change in wavelength between two adjacent wavy units, and similarly for the amplitude. Their study found that $\Delta\lambda = 400\ \mu$m and $\Delta A = 8\ \mu$m was the optimal combination.

As the power dissipation of microprocessors continues to increase, different methods of on-chip MCHS have been investigated to reduce and thermal resistance due to the interface between the convective cooling medium and the heat-generating chip [14]. Data centers are home to hundreds of servers that contain many electrical components including processing chips. The need to build more energy-efficient data centers has been brought to light over the years as the data center industry is currently responsible for 1.3% of the worlds electricity

consumption [15]. For a typical data center, roughly 38% of its power consumption is allocated for the cooling systems so integrating MCHS into processor cooling systems can have a huge impact in reducing the power consumption of data centers [15].

1.2 Objective

This study is designed to assess the hypothesis that increasing or decreasing the wavelength along the direction of flow will enhance the heat transfer performance for both up-down and left-right wavy microchannel heat sinks. Up-down and left-right will be referred to as vertical wavy and horizontal wavy, respectively, in this present study. This hypothesis will be tested by comparing the Nusselt number, bottom wall temperature difference, and thermal resistance of vertical and horizontal wavy MCHS with increasing or decreasing wavelengths to those of the straight channel. This comparison will aid in determining if more complex wavy MCHS are worth pursuing for better heat transfer performance than straight MCHS. A fair comparison can be made between the straight, vertical wavy, and horizontal wavy designs since the projected channel length in x-direction will be the same while the arc length of the channel path will have a negligible difference. The higher heat transfer effect for both designs is expected due to the increased quantity of vortices produced within the flow. The bottom wall temperature difference, Nusselt number, and thermal resistance are the performance indicators that will be examined to determine a superior design.

This study was partially inspired by the work of Lin et al. [13], who investigated horizontal wavy MCHS at simultaneous varying amplitude and wavelength. This present study will computationally investigate both horizontal and vertical wavy designs with

simultaneous varying amplitude and wavelength. Studying different wavelengths and amplitudes will provide insight to an optimal combination for vertical and horizontal wavy MCHS designs.

2 METHODOLOGY

2.1 Model Validation

The present CFD model has been validated using the published experimental data for the friction factor and the Nusselt number from Sui et al. [7]. The experimental results were obtained for a horizontal wavy sinusoidal MCHS with a constant amplitude of 138 μm and a constant wavelength of 2500 μm at Reynolds number of 300-800 varying by 100. The sinusoidal wave can be constructed using Equation 1 where A is the amplitude and λ is the wavelength. The materials chosen for the solid and liquid are copper and water, respectively, and their thermophysical properties are shown in Table 1 at room temperature of 293 Kelvin.

$$y = Acos(2\pi x/\lambda) \tag{1}$$

Table 1
Thermophysical Properties of the Solid and Fluid Used

Material	Density (kg /m^3)	Cp (J/ kg K)	k (W /m K)	μ (kg/ m s)
Coolant: Water	998.2	4182	0.6	0.001003
Solid: Copper	8978	381	387.6	--

2.2 Model Validation – Geometry

The geometry studies by Sui et al. [7] has a constant channel profile that spans along the length of the MCHS with a total of ten wavelengths. The geometric parameters for this MCHS are listed in Table 2 below. The hydraulic diameter is calculated using Equation 2 which is for a rectangular duct with all four sides of the duct considered as the wetted perimeter, where a is the height and b is the width [16].

$$D_h = \frac{2ab}{a+b} \tag{2}$$

Table 2
Geometric Parameters of Wavy MCHS Studied by Sui et al. [7]

$H_c\ (\mu m)$	$W_c\ (\mu m)$	$S_r\ (\mu m)$	$S_b\ (\mu m)$	$D_h\ (\mu m)$	$L_c\ (\mu m)$	$A\ (\mu m)$	$\lambda\ (\mu m)$
406	207	96.5	96.5	262.96	25000	138	2500

The geometry was created in SOLIDWORKS using a function curve in the form of Equation 1 and off-setting additional curves by the thickness of the ribs, S_r, and channel width, W_c, and extruding the base and the ribs to the height of the base, S_b, and the channel height, H_c, respectively. The complete 3D model is shown in Fig. 1.

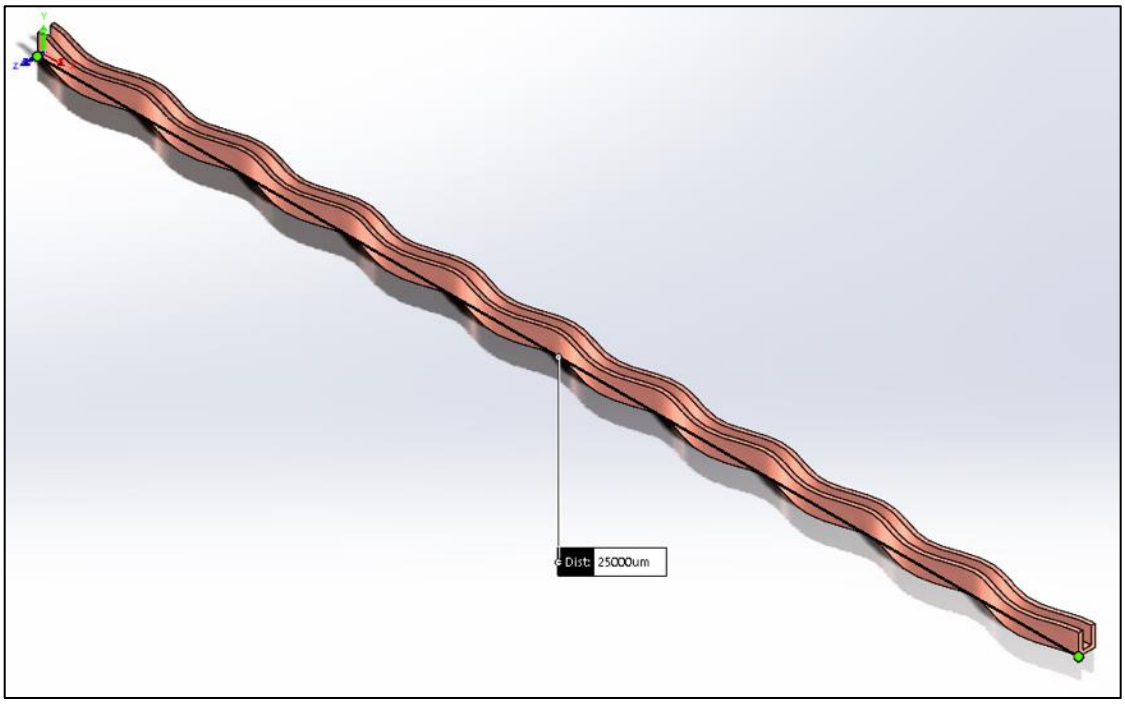

Fig. 1. Geometry of single wavy channel of 3D model from Sui et al. [7] experiments.

The experimental setup of Sui et al. [7] included an inlet entrance region before entering the channel. This region was not fully described in this study, so two methods were explored to replicate the entrance region. The first method was to extend the wavy region of the inlet by half the length of the channel as shown in Fig. 2. The second method displayed in Fig. 3

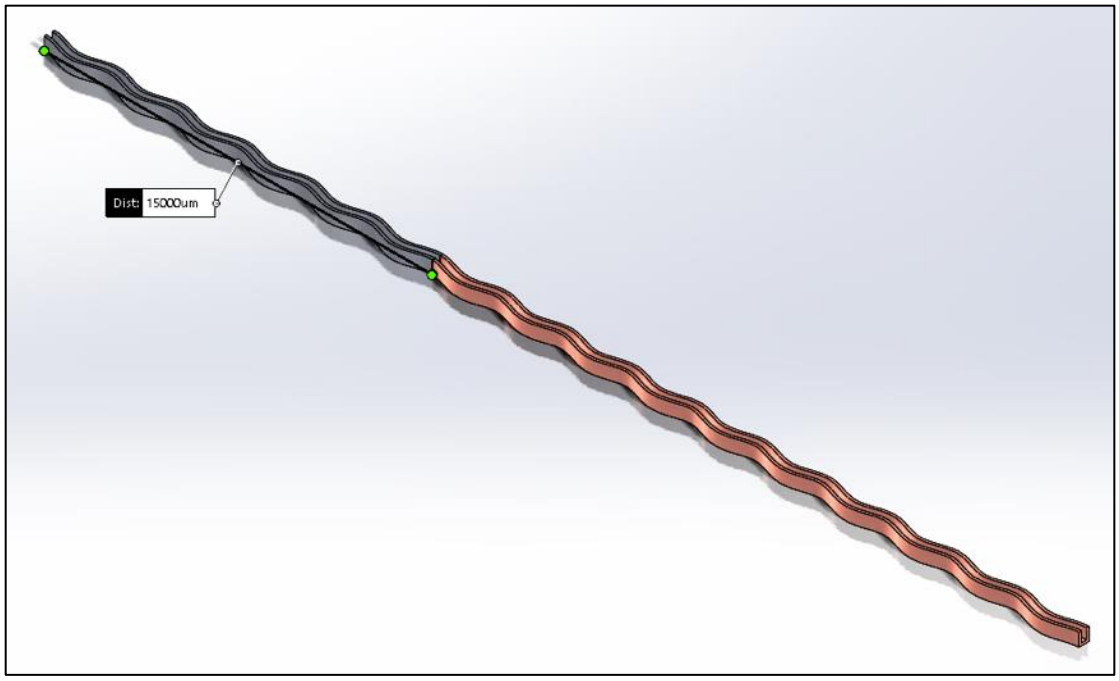

Fig. 2. Geometry of single wavy channel with extended wavy inlet.

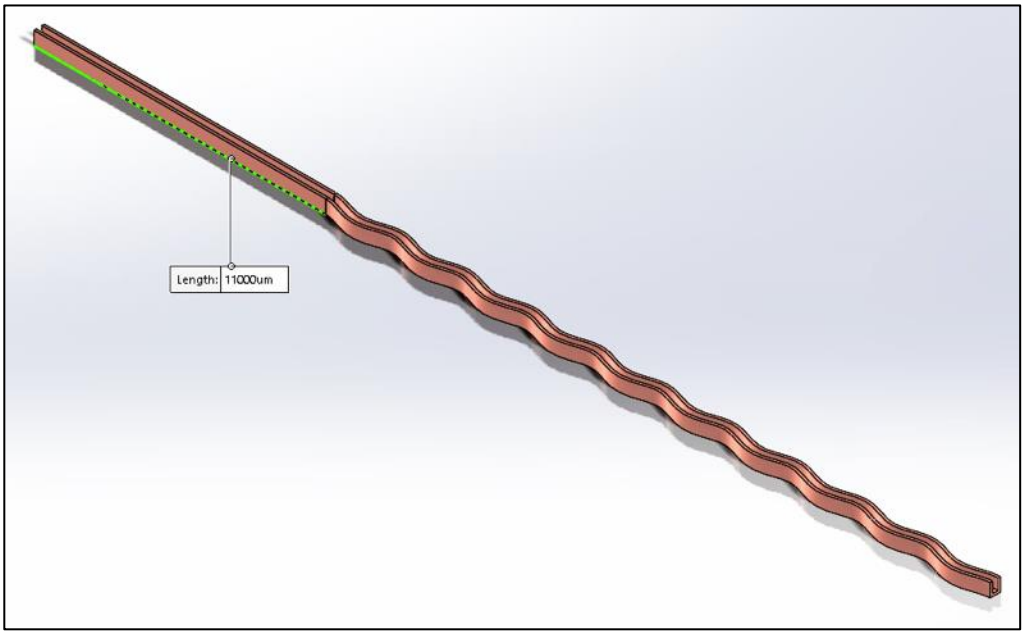

Fig. 3. Geometry of single wavy channel with extended straight inlet.

included extending the inlet with a straight channel using the hydrodynamic entrance length for laminar flow described in Equation 3 [16] to initiate fully developed flow entering the MCHS.

$$L_{h,laminar} = 0.05ReD_h \quad (3)$$

2.3 Model Validation – Meshing

Three mesh sizes were selected to conduct a grid independence study to determine if the mesh resolution had any effect on the accuracy of the result. The coarse, medium, and fine meshes used in Zhu et al. [12] and Lin et al. [13] were initially used as reference points when selecting the number of fluid nodes for the meshes in the present study due to the similarity in geometries and CFD models and were varied slightly to produce three new mesh sizes. The three mesh sizes are shown in Table 3. The total number of fluid nodes were considered more significant in determining the mesh size than the number of solid nodes because there are more governing equations that are solved in the fluid nodes which will significantly affect the total time for computation. The average computational time for the medium mesh took roughly 18 minutes longer than the coarse mesh, but the fine mesh clocked in at over an hour longer than the medium mesh.

Table 3
Mesh Sizes and Computational Time

	Coarse	**Medium**	**Fine**
x-direction	150	300	450
y-direction	30	40	50
z-direction	35	45	55
Fluid Nodes	157500	540000	1237500
Total Nodes	171168	570338	1290708
Average Time (minutes)	5.26	23.94	107.44

The criteria examined for the mesh quality is aspect ratio, skewness, and orthogonality, and Table 4 includes the maximum, average, and minimum of each criterion for all three meshes. The criteria used in this study was referenced from the "Introduction to ANSYS Fluent" lecture [17] which suggested a skewness less than 0.95, orthogonality greater than 0.1, and aspect ratio less than 100 which are met by all three mesh sizes.

Table 4
Mesh Quality Criteria for All Meshes

	Coarse			Medium			Fine		
Metric	Min.	Avg.	Max.	Min.	Avg.	Max.	Min.	Avg.	Max.
Aspect Ratio	8.45	24.62	25.16	8.45	16.78	16.5	8.45	13.76	14.14
Skewness	2.03E-04	0.14	0.24	1.29E-03	0.14	0.31	1.06E-04	0.14	0.37
Orthogonality	0.87	0.96	0.99	0.88	0.97	0.99	0.85	0.99	0.97

2.4 Model Validation – Simulation

The commercial CFD software Ansys Fluent which uses the finite volume method (FVM) was selected for this study with the standard SIMPLE (Semi-implicit method for pressure-linked equation) scheme for pressure-velocity coupling. The convergence criteria were set to 1e-6 for all equations to ensure accurate results for the model containing single-phase flow. Fig. 4 shows that a tight convergence of 1e-6 was met by all equations, and no large positive slope is seen that would have resulted in divergence. The laminar viscous model is used due to very low Reynolds numbers for internal flow.

The governing equations for thermal and fluid flow including the continuity, momentum, and energy equation, and also the energy equation for a solid are solved simultaneously. These governing equations [16] are shown in Equations 4 through 9. Assumptions have been made to reduce the number of terms and simplify the equations. These assumptions include steady-state, laminar flow, incompressible flow, and constant viscosity.

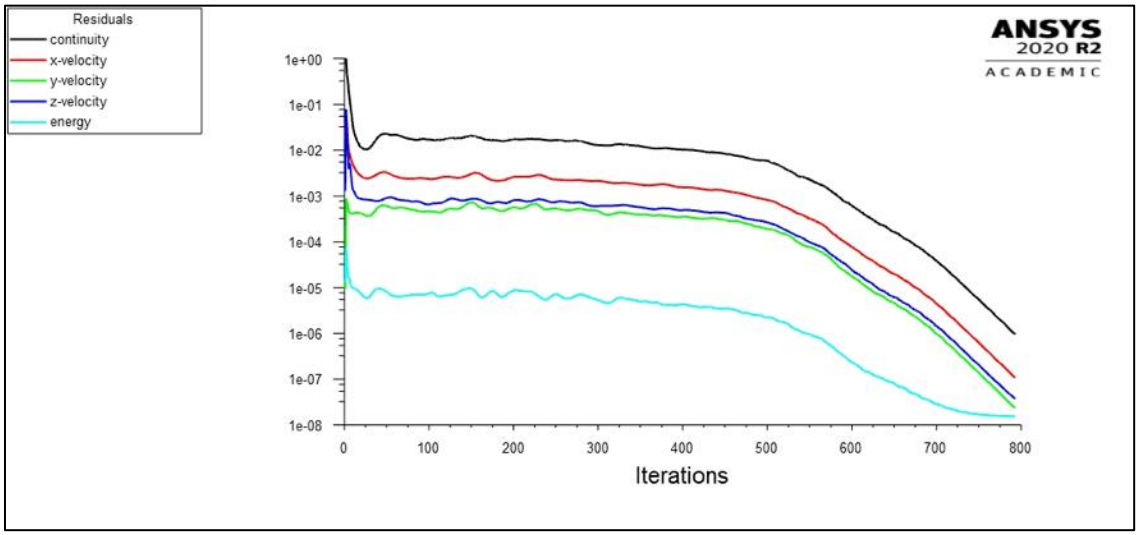

Fig. 4. Normalized residuals vs. iterations at Re = 800 for coarse mesh.

Continuity equation:

$$\frac{\partial u}{\partial x} + \frac{\partial v}{\partial y} + \frac{\partial w}{\partial z} = 0 \tag{4}$$

Here, *u*, *v*, and *w* are the corresponding *x*, *y*, and *z* velocity components, respectively, given by. This equation demonstrates that mass is conserved.

Momentum equations:

$$\rho\left(\frac{\partial u}{\partial t} + u\frac{\partial u}{\partial x} + v\frac{\partial u}{\partial y} + w\frac{\partial u}{\partial z}\right) = -\frac{\partial p}{\partial x} + \mu\left(\frac{\partial^2 u}{\partial x^2} + \frac{\partial^2 v}{\partial x^2} + \frac{\partial^2 w}{\partial x^2}\right) + \rho g_x \tag{5}$$

$$\rho\left(\frac{\partial v}{\partial t} + u\frac{\partial v}{\partial x} + v\frac{\partial v}{\partial y} + w\frac{\partial v}{\partial z}\right) = -\frac{\partial p}{\partial y} + \mu\left(\frac{\partial^2 u}{\partial y^2} + \frac{\partial^2 v}{\partial y^2} + \frac{\partial^2 w}{\partial y^2}\right) + \rho g_y \tag{6}$$

$$\rho\left(\frac{\partial w}{\partial t} + u\frac{\partial w}{\partial x} + v\frac{\partial w}{\partial y} + w\frac{\partial w}{\partial z}\right) = -\frac{\partial p}{\partial z} + \mu\left(\frac{\partial^2 u}{\partial z^2} + \frac{\partial^2 v}{\partial z^2} + \frac{\partial^2 w}{\partial z^2}\right) + \rho g_z \tag{7}$$

Here, ρ is the density, $\frac{\partial p}{\partial x}$ is the pressure gradient in the *x*-direction, μ is the viscosity, and g_i is the gravitational acceleration in the *i*-direction. The physical principle of these equations is that momentum is conserved, similarly to Newton's second law equating force to mass multiplied by acceleration.

Energy equation for the fluid:

$$\rho C_p\left(\frac{\partial T}{\partial t}+u\frac{\partial T}{\partial x}+v\frac{\partial T}{\partial y}+w\frac{\partial T}{\partial z}\right)=\frac{\partial}{\partial x}\left(k\frac{\partial T}{\partial x}\right)+\frac{\partial}{\partial y}\left(k\frac{\partial T}{\partial y}\right)+\frac{\partial}{\partial z}\left(k\frac{\partial T}{\partial z}\right)+$$

$$\left(\frac{\partial p}{\partial t}+u\frac{\partial p}{\partial x}+v\frac{\partial p}{\partial y}+w\frac{\partial p}{\partial z}\right)+\mu\Phi+\dot{q} \quad (8)$$

Where $\Phi = 2\left[\left(\frac{\partial u}{\partial x}\right)^2+\left(\frac{\partial v}{\partial y}\right)^2+\left(\frac{\partial w}{\partial z}\right)^2\right]+(\frac{\partial v}{\partial x}+\frac{\partial u}{\partial y})^2+(\frac{\partial w}{\partial y}+\frac{\partial v}{\partial z})^2+(\frac{\partial u}{\partial z}+\frac{\partial w}{\partial x})^2-$

$$\frac{2}{3}(\frac{\partial u}{\partial x}+\frac{\partial v}{\partial y}+\frac{\partial w}{\partial z})^2$$

Here, C_p is the specific heat at constant pressure, T is the temperature, k is the thermal conductivity, $\dot{q}$ is the heat generation per unit volume which is 0 for this study. This equation demonstrates that energy is conserved within any fluid flow.

Energy equation for the solid:

$$\frac{\partial}{\partial x}\left(k\frac{\partial T}{\partial x}\right)+\frac{\partial}{\partial y}\left(k\frac{\partial T}{\partial y}\right)+\frac{\partial}{\partial z}\left(k\frac{\partial T}{\partial z}\right)=0 \quad (9)$$

This equation demonstrates that energy is conserved with any solid via conduction heat transfer.

The parameters studied in this model validation include the friction factor and Nusselt number. The friction factor shown in Equation 10 will vary from case to case based on the pressure drop, $\frac{dp}{dx}$, and velocity of the flow. The average heat transfer coefficient is calculated using Equation 11 where $A_b$is the area of the base where the heat flux is applied, N is the # of channels which is one for this study, A_w is the area for convection on the channel walls, T_w is the average channel temperature, and T_m is the mean temperature of the fluid described as Equation 13 [18], [19] where T_{in} and T_{out} are the inlet and outlet temperature of the fluid, respectively. The average Nusselt number is defined as Equation 14 [18].

$$f = -[(\frac{dp}{dx})\left(\frac{2D_h}{\rho U^2}\right)] \quad (10)$$

$$h_m = \frac{q_w A_b}{N A_w (T_w - T_m)} \quad (11)$$

$$A_w = (2H_c + W_c)L_x \quad (12)$$

$$T_m = \frac{(T_{in} + T_{out})}{2} \quad (13)$$

$$Nu = \frac{h_m D_h}{k_f} \quad (14)$$

The boundary conditions for this model are as follows (see Fig. 5):

Inlet of the microchannel: $u = u_{in}, v = 0, w = 0, T = T_{in} = 300\ K$

Outlet of the microchannel: $p = p_{out}$

Bottom wall of the heatsink: $q_w = -k_s \frac{\partial T_s}{\partial n} = constant = 50\ {}^{W}/_{cm^2}$

Solid and fluid interfaces: $u = 0, v = 0, w = 0, k_f \nabla T_f = k_s \nabla T_s$

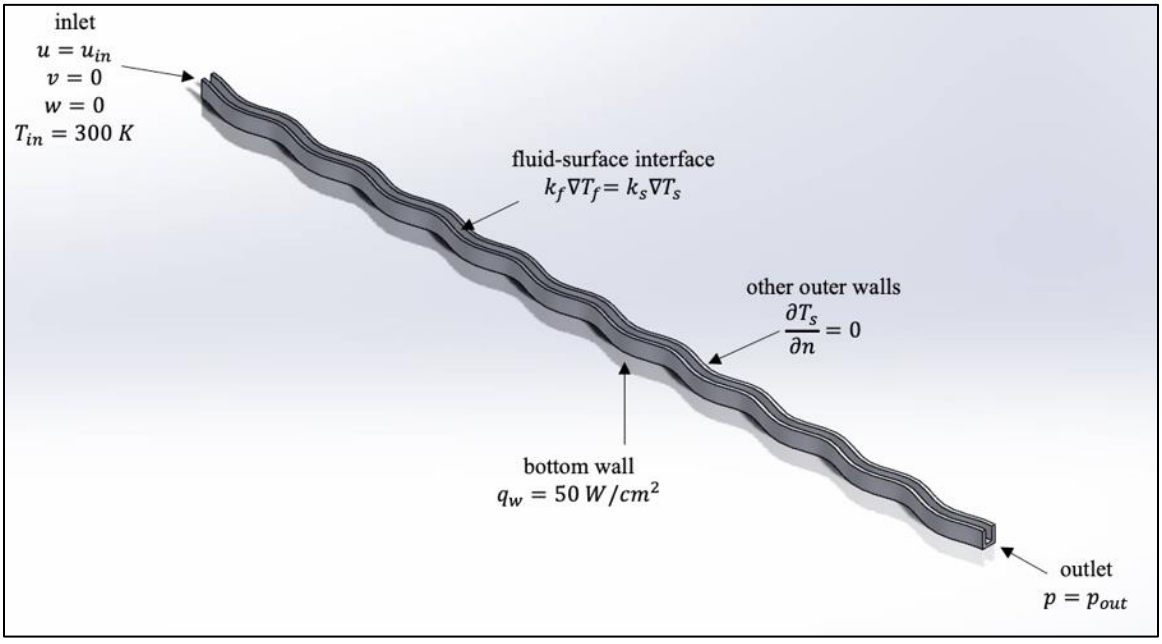

Fig. 5. Boundary conditions imposed on CFD model for model validation.

2.5 Simulation Method

Similar to the model validation case, Ansys Fluent is used conduct the CFD simulations for this study, but instead of only using the standard SIMPLE scheme for pressure-velocity coupling, the coupled scheme is deployed for better convergence results. The convergence criteria were set to 1e-6 for all governing equations. Typical normalized residuals are displayed in the Fig. 6 which shows tight convergence. The coolant for these simulations is water and the solid is silicon and their thermophysical properties are shown in Table 5.

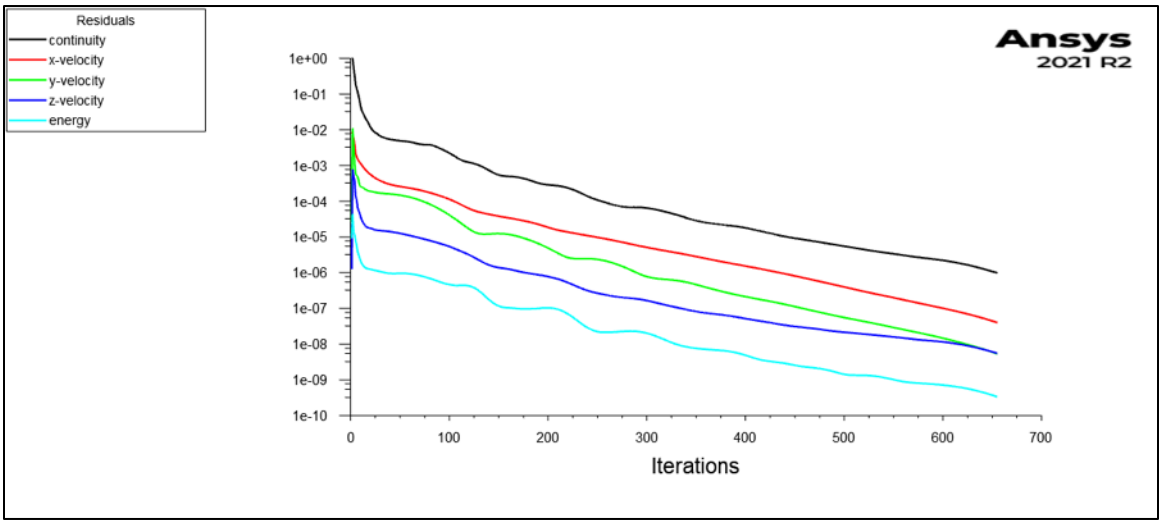

Fig. 6. Normalized residuals vs. iterations for vertical wavy MCHS with constant amplitude and constant wavelength at Re = 500

Table 5
Thermophysical Properties of the Solid and Fluid Used

Material	Density (kg /m^3)	Cp (J/ kg K)	k (W /m K)	μ (kg/ m s)
Coolant: Water	998.2	4182	0.6	0.001003
Solid: Silicon	2329	702	124	--

The boundary conditions that are used for the following simulations are shown in Fig. 7 and are nearly identical to those used in the model validation except the constant heat flux applied at the bottom wall is now 100 W/cm^2.

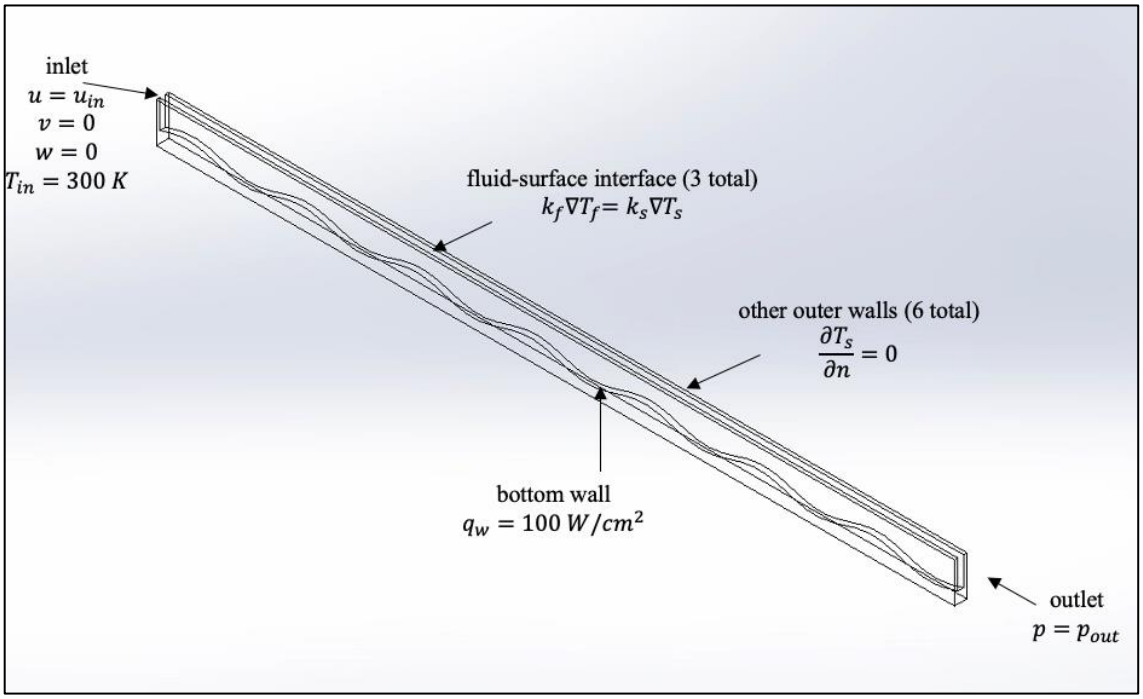

Fig. 7. Boundary conditions imposed for the CFD simulations.

2.6 Geometric Design

All of the 3D models will be created in SOLIDWORKS software. A single wavy unit is shown in Fig. 8. A wavy unit can be created simply by knowing the wavelength and amplitude connecting the points using the arc feature. There will be seven wavy units in total for each MCHS.

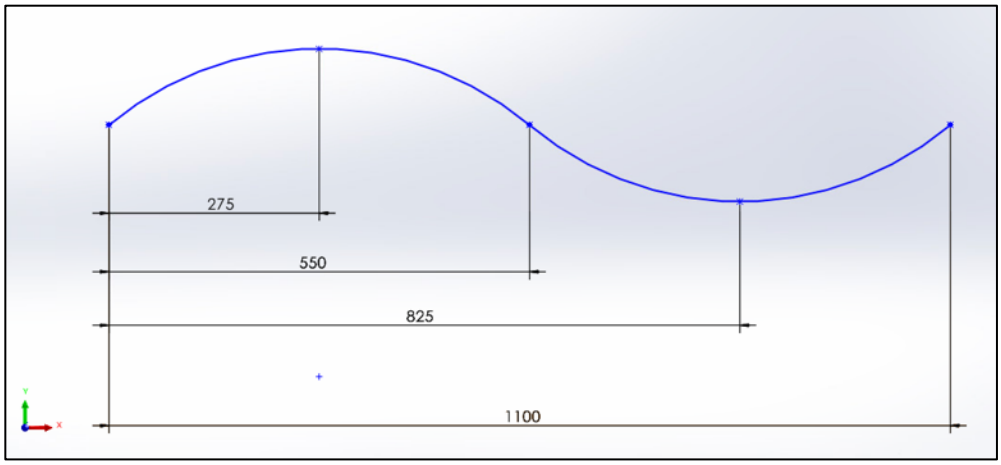

Fig. 8. One wavy unit with A = 100 μm and λ = 1000 μm.

For the cases that are varying in wavelength, $\Delta\lambda$, along the flow direction, an arithmetic progression method proposed by Lin et al. [13] will be used. The cases examined with varying wavelength are $\Delta\lambda$ = 150 μm, 300 μm. The wavelength or amplitude will change in the following fashion:

- $\lambda_{i+1} - \lambda_i = \Delta\lambda$ for i = 1,2,3,4,5,6
  - e.g. if $\Delta\lambda$ = 300 μm and λ_1 = 1100 μm, then $\lambda_2 = 1400$ μm, etc. (shown in Figure 4)

An example of one wavy unit with a wavelength of 1100 is shown in Fig. 8. Seven wavy units varying in wavelength with $\Delta\lambda = 300$ μm is shown in Fig. 9. It should be stated that the fourth wavy unit for each geometry is 2000 μm, and the projected (straight) length of each geometry is 14000 μm. It should also be noted that for a case with $\Delta\lambda = 150$ μm the wavelength is increasing in the flow direction, and for a case with $\Delta\lambda = -150$ μm the wavelength is decreasing in the flow direction.

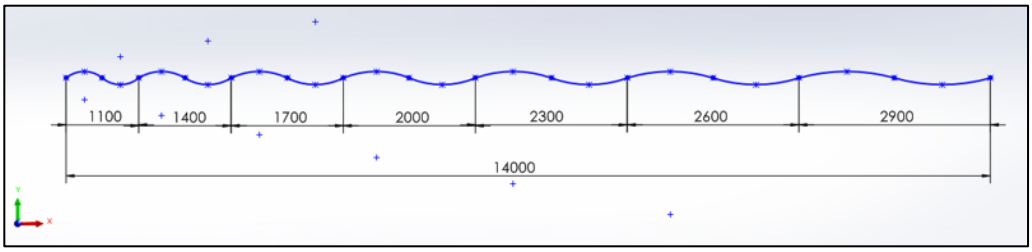

Fig. 9. Seven wavy units with $\Delta\lambda = 500$ μm and ΔA = -25 μm.

The constant geometric parameters for the MCHS in this study are listed in Table 6. The channel cross-section area and its respective parameters are shown in Fig. 10. The aspect ratio for all geometries in this study is 5, which was selected based on high performance of vertical wavy MCHS with an aspect ratio of 5 by Zhu et al. [12]. Fig. 11 and Fig. 12 provided one case of geometries that is studied for vertical and horizontal wavy MCHS, respectively.

Table 6
Constant Geometric Parameters of Wavy MCHS

H_c (μm)	W_c (μm)	S_r (μm)	S_b (μm)	D_h (μm)	L_c (μm)
500	100	60	200	166.67	14000

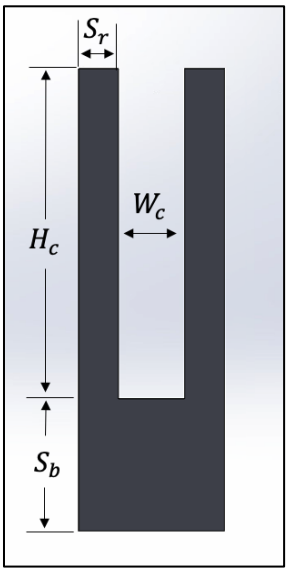

Fig. 10. Channel profile of wavy MCHS geometries.

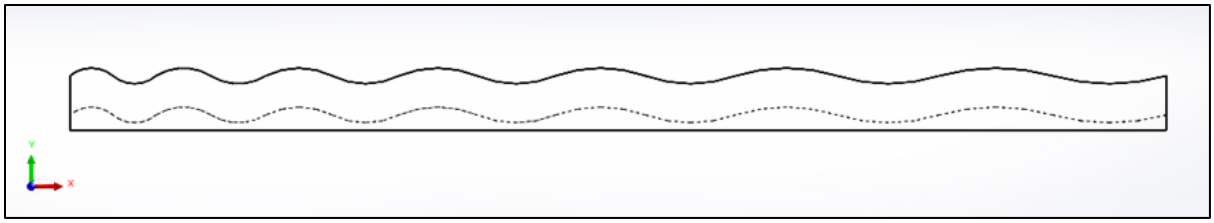

Fig. 11. x-y plane (side) view of vertical wavy MCHS with A = 100 μm and $\Delta\lambda$ = 300 μm.

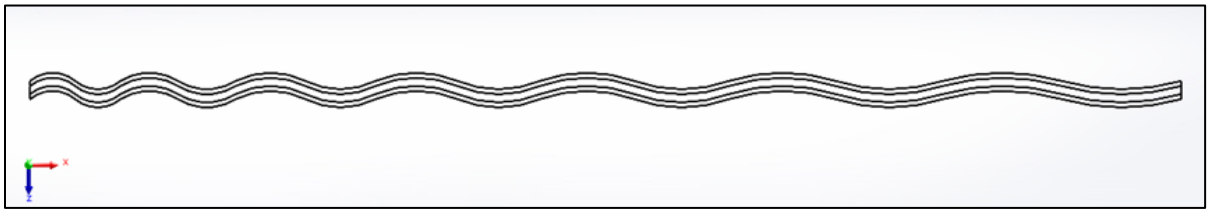

Fig. 12. x-z plane (top) view of horizontal wavy MCHS with A = 100 μm and $\Delta\lambda$ = 300 μm.

3 RESULTS AND DISCUSSION

3.1 Model Validation – Results

The Nusselt number and friction factor were obtained via CFD simulations for Reynolds number ranging from 300-800, with an increment step of 100. The results for the friction factor are displayed in Fig. 13. These results show good agreement with those of Sui et al. [7] as the experimental uncertainty for the friction factor was listed at 3%. The results for the Nusselt number are shown in Fig. 14 and convey an overall agreeable trend with the experimental data that listed an uncertainty of 18%. This difference may be due to the density and viscosity of water for the experiments being measured at the mean fluid temperature. The largest difference in results occurs at lower Reynolds numbers of 300 and 400. This difference can be due to a couple of reasons. Firstly, the experiments could have been able to completely capture the inlet temperature at 300 K which would result in a small difference of mean temperature and heat transfer coefficient. Second, the inlet velocity condition of the experiments isn't explicitly explained, so a small deviation in velocity could affect the heat transfer performance. For these simulation results there is no identifiable mesh dependency, so the coarse mesh was used for the following simulations to reduce the computational time.

Dean vortices develop in the *y-z* plane along the channel and change in size and location significantly along the flow direction throughout the peaks and troughs of the waves. Three 2D plane slices are created to display the flow fields at the front in Fig. 15, the middle in Fig. 16, and the end in Fig. 17, all within the sixth wavelength. The flow fields appear to be symmetric at about the mid-plane of the channel height. This is due to the two walls on

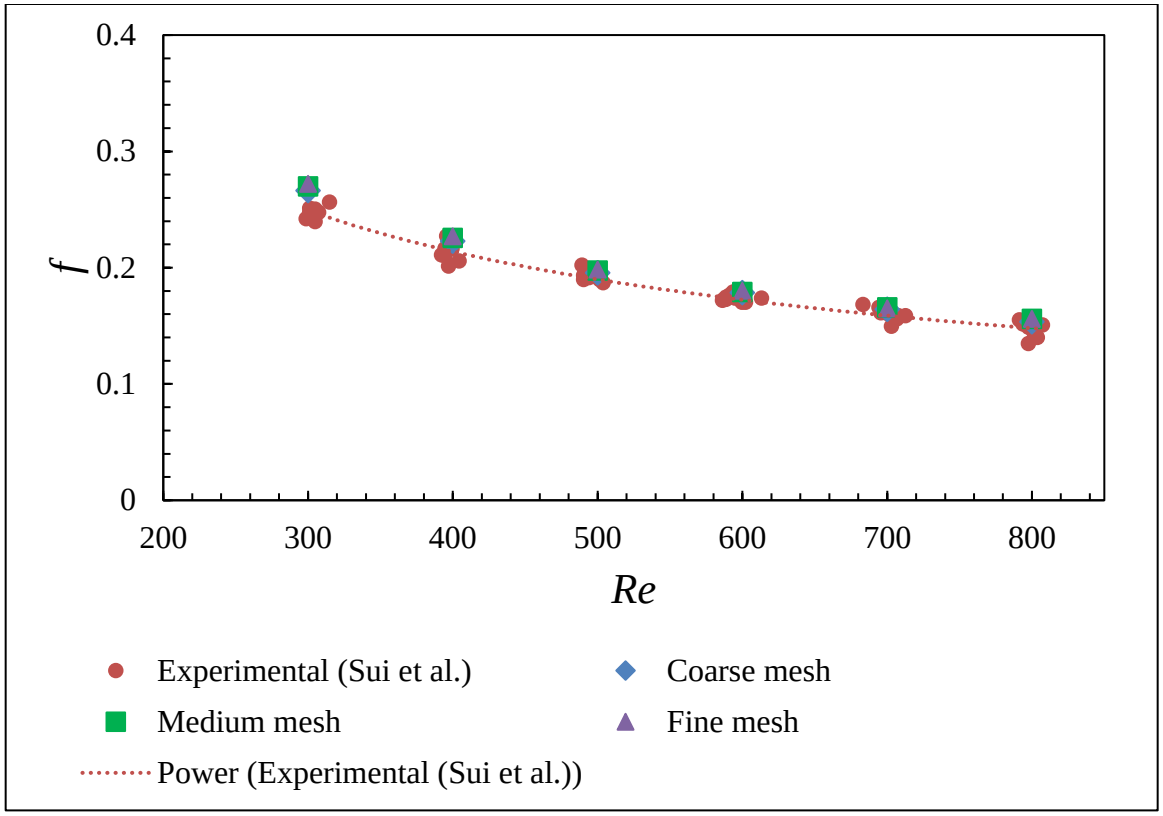

Fig. 13. Comparison of friction factors with experimental data from Sui et al. [7] with power trendline.

top and bottom enclosing the flow and the symmetry of the channel about the mid-plane of the channel height. No vortices are produced in the lateral direction which likely because of the small amplitudes of the MCHS.

As mentioned above in the *Model Validation – Geometry* section, two methods were adopted to replicate fully developed flow entering the inlet of the channel. Table 7 lists the friction factor and Nusselt numbers for all inlet cases at the extreme flow rates corresponding to Re = 300 and Re = 800 for the coarse mesh. The results are very similar for the friction factor for all three cases, but both of the extended inlet cases produced a slightly larger

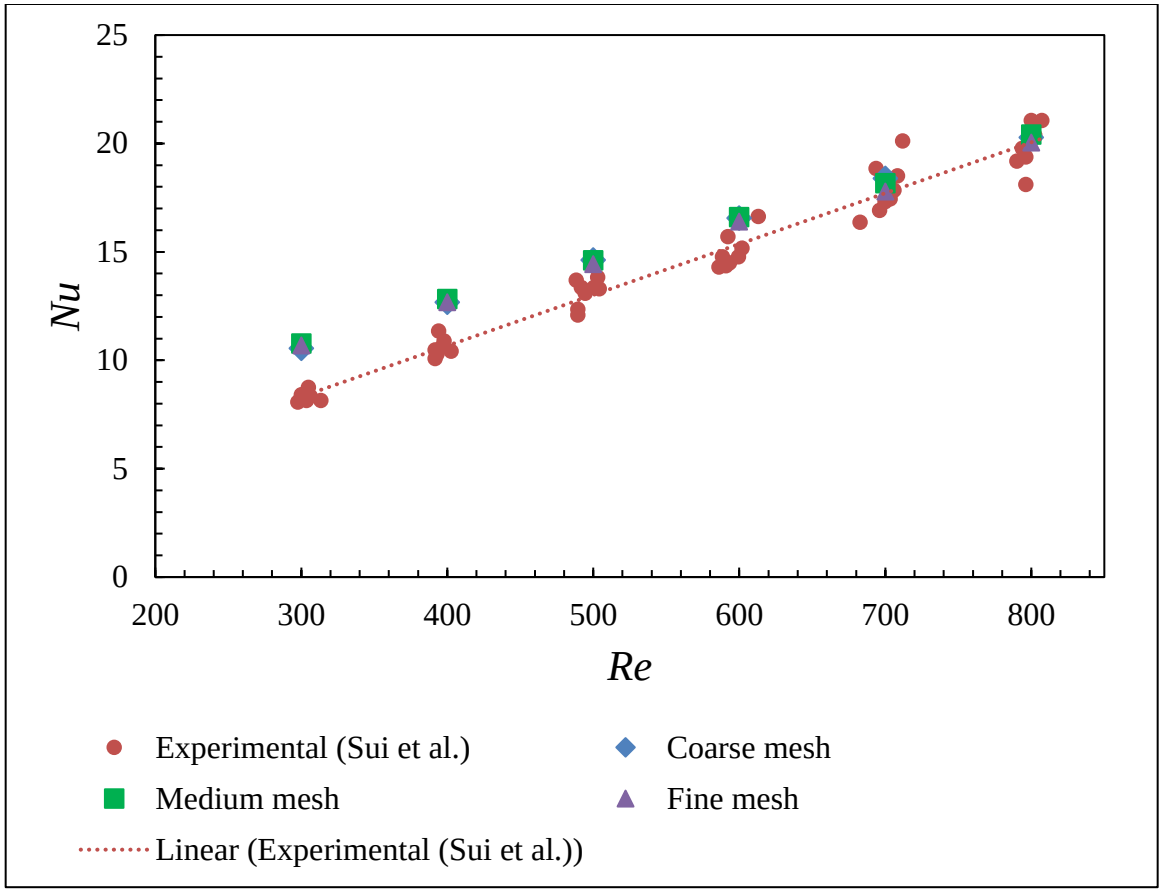

Fig. 14. Comparison of Nusselt numbers with experimental data from Sui et al. [7] with linear trendline.

Nusselt number. This is not completely intuitive as the difference between the wall temperature, T_w, and the mean fluid temperature, T_m, is smaller in the entrance region for a pipe at constant heat flux resulting in a higher heat transfer coefficient, but the difference grows and becomes constant once fully developed flow is reached [20]. This will need to be further investigated to ensure there were no heat losses into the extended inlet section which would result in a slightly lower wall temperature, and thus a slightly higher Nusselt number.

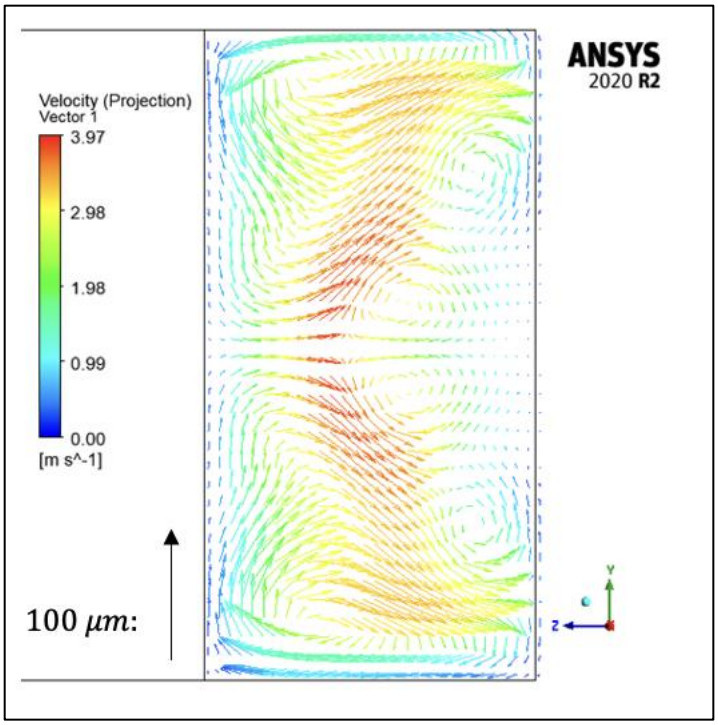

Fig. 15. Velocity vectors along z-y plane of wavy MCHS at x = 5λ.

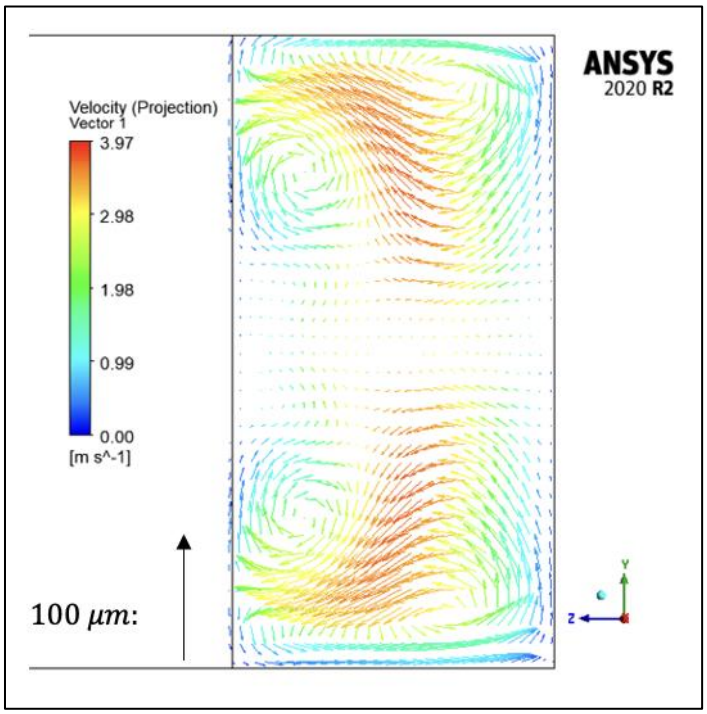

Fig. 16. Velocity vectors along z-y plane of wavy MCHS at x = 5.5λ.

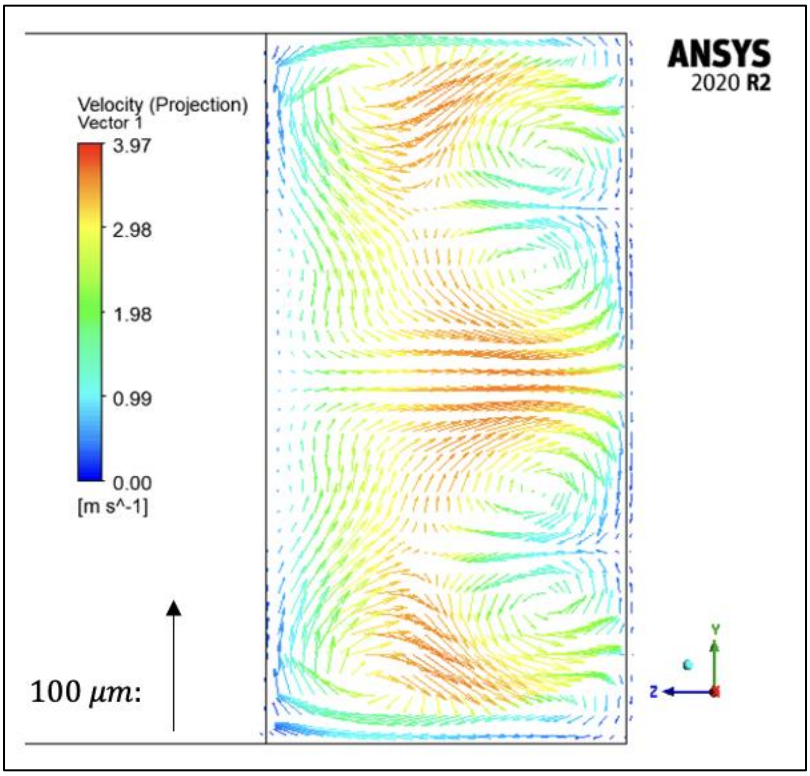

Fig. 17. Velocity vectors along z-y plane of wavy MCHS at x = 6λ.

Table 7
Friction Factor and Nusselt Number at Re = 300 and Re = 800 for All Inlet Cases With Coarse Mesh

	f		Nu	
Inlet type	Re = 300	Re = 800	Re = 300	Re = 800
Uniform velocity inlet	0.267	0.154	10.8	20.8
Extended wavy inlet	0.271	0.157	11.1	21.0
Extended straight inlet	0.264	0.152	11.1	20.8

3.2 Simulation Results – Constant Amplitude and Constant Wavelength

Simulations were conducted for the vertical wavy and horizontal wavy design with a constant amplitude of A = 100 μm and λ = 2000 at Re of 100, 200, 300, 400, 500. These two designs were compared to the straight channel case to see if the heat transfer performance

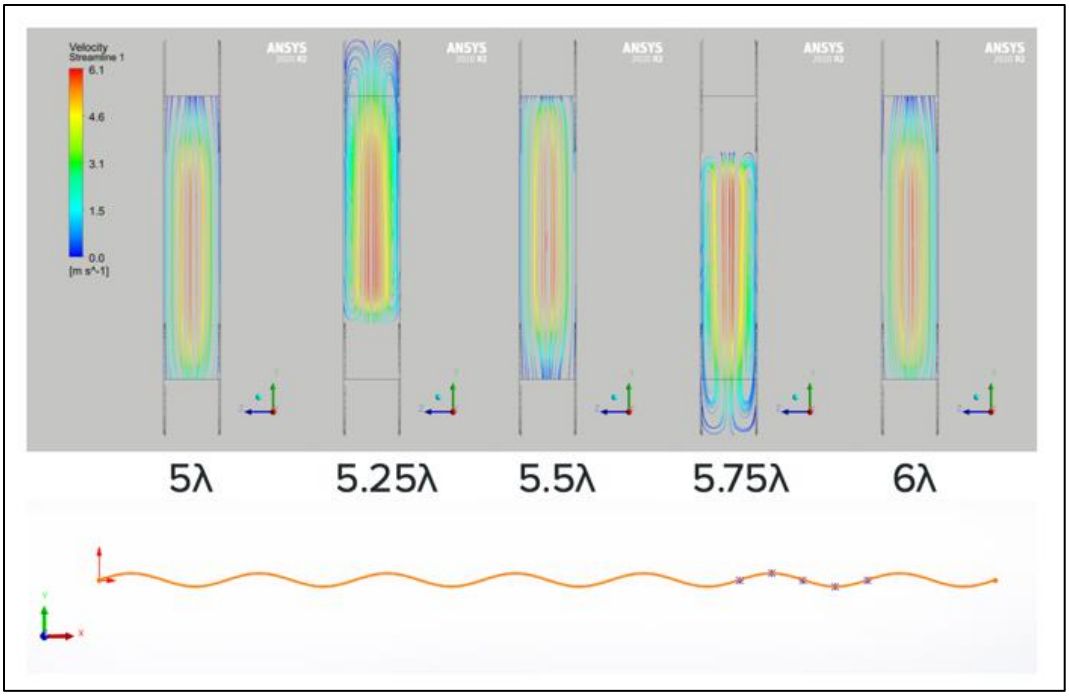

Fig. 18. Y-Z plane velocity streamlines at x = 5λ, 5.25λ, 5.5λ, 5.75λ, 6λ for the vertical wavy design with A = 100 μm and λ = 2000 μm at Re = 500.

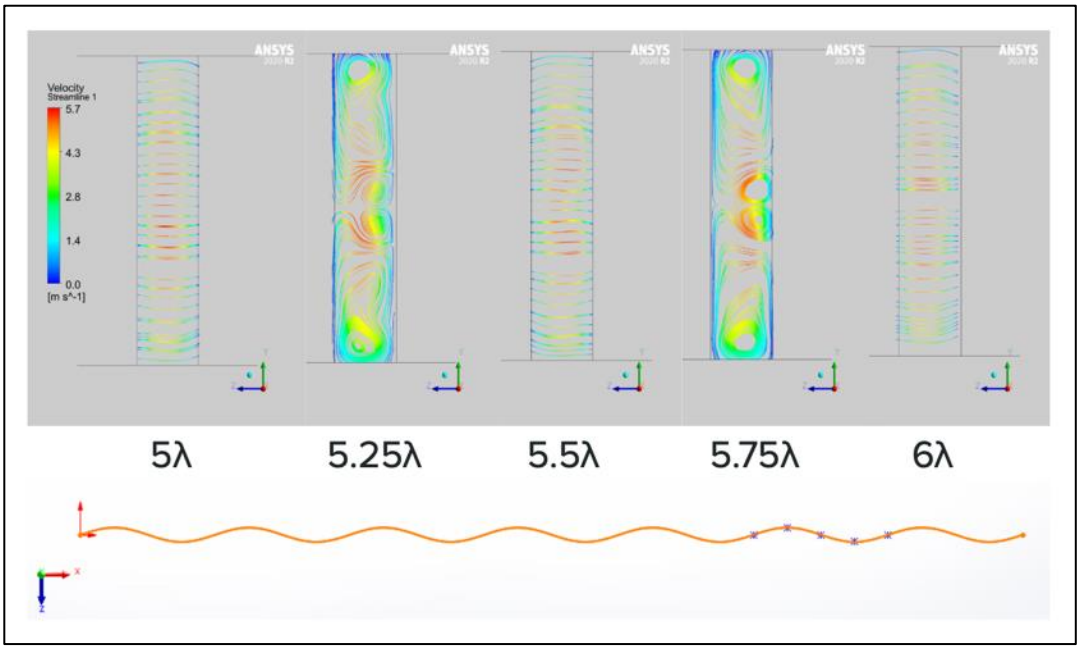

Fig. 19. Y-Z plane velocity streamlines at 5λ, 5.25λ, 5.5λ, 5.75λ, 6λ for the horizontal wavy design with A = 100 μm and λ = 2000 μm at Re = 500.

was better. Velocity streamlines are shown in Fig. 18 and Fig. 19 for the vertical and horizontal wavy designs, respectively. It can be seen that in the peaks and troughs of the vertical wavy design there are two long symmetrical vortices that form along the sides of the channel and run vertically in the z-direction. These vortices can create some mixing but are hindered and not able to grow any larger in width due to the slenderness of the channel width. In Fig. 19 it can be seen that symmetrical vortices are also produced in the flow of the horizontal wavy design. There are four vortices in total and are symmetrical amongst the midpoint of the channel in the z-direction. These vortices are able to produce a lot of mixing and in different regions of the 2D-plane of the channel which helps with the overall cooling of the fluid.

Temperature contours for the all cases are shown in Fig. 20. The straight channel has a large blue region of cool temperature for the fluid and absorbs more heat as it travels through the length of the channel with no mixing that occurs. The blue region is slightly smaller for the vertical wavy design, but it can be seen that the coolant near the bottom wall of the channel has a much higher temperature. This may be due to this location being at a trough of the vertical wavy design which by the nature of the design has less solid material between the bottom wall of the channel and the bottom wall of the heat sink, so the fluid will be closer to where the heat flux is applied. The horizontal wavy design produced adequate mixing and the blue region is noticeably smaller due the heat dissipating better throughout the coolant.

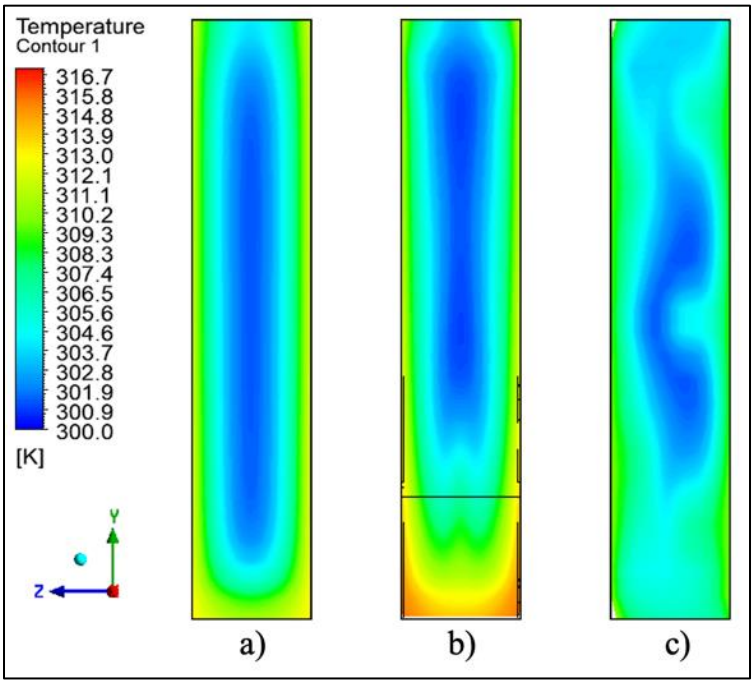

Fig. 20. Temperature contour of fluid along y-z cross section at x = 5.75λ for (a) straight, (b) vertical, and (c) horizontal with A = 100 μm and λ = 2000 μm.

The results for the Nusselt number are shown in Fig. 21. The straight and vertical wavy design both performed similarly but at Re of 300 and higher the straight channel begins to yield a slightly higher Nu. The horizontal wavy design underperforms for Re of 100 and 200, but follows a linear trend and has a much higher Nu then both the straight and vertical designs at Re of 400 and 500.

The pressure drop comparison is shown in Fig. 22, and it can be seen that the straight design produces a smaller pressure drop than the vertical and horizontal wavy designs. This is mainly because the path traveled by the straight channel is slightly shorter than the path traveled by the wavy designs as the follow the arc lengths of the sinusoidal wave. Fig. 23 displays the maximum temperature difference along the bottom wall which shows that similar to the Nu, the horizontal wavy design underperforms compared to the straight and

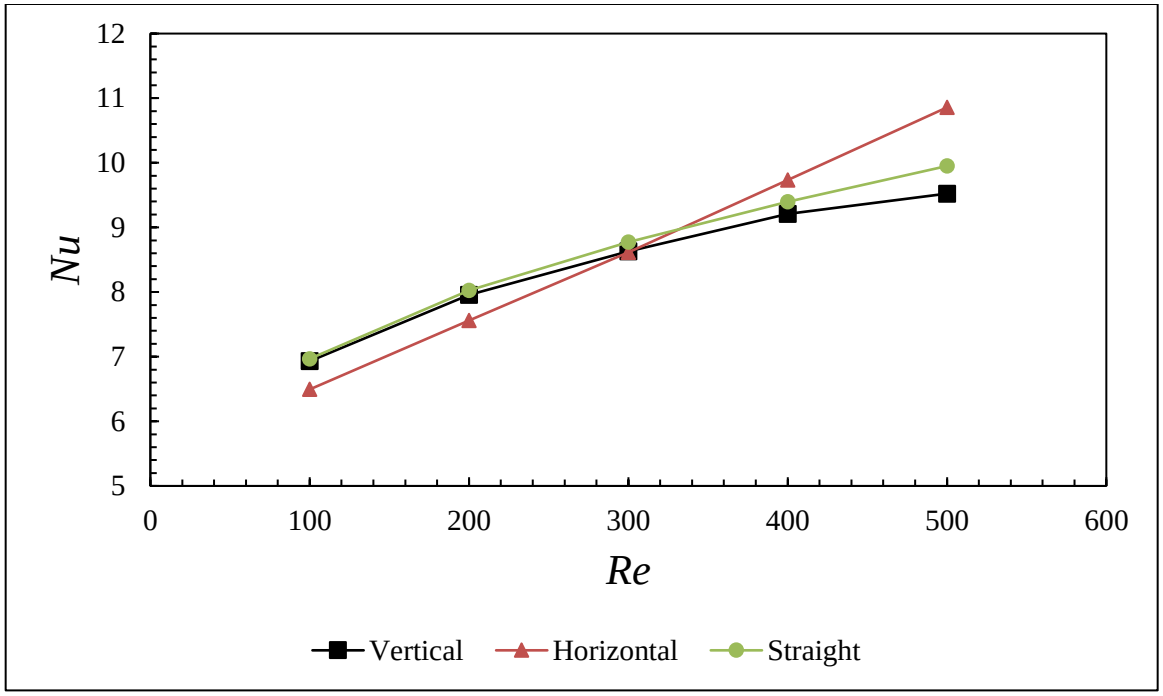

Fig. 21. Nusselt number of straight, vertical, and horizontal wave MCHS with A = 100 μm and λ = 2000 μm.

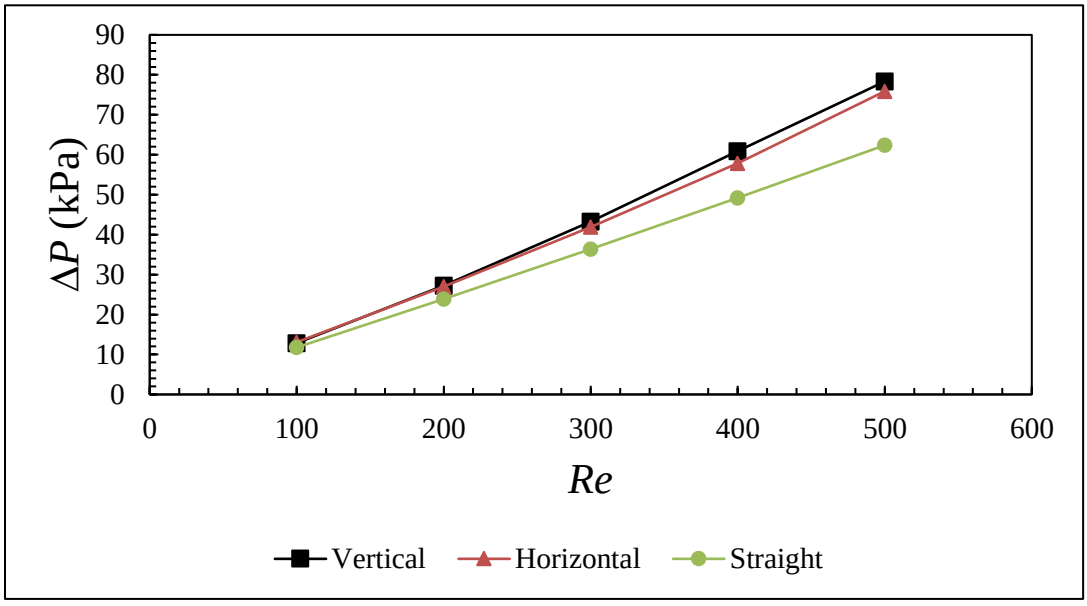

Fig. 22. Pressure drop across the heatsinks for straight, vertical, and horizontal wave MCHS with A = 100 μm and λ = 2000 μm.

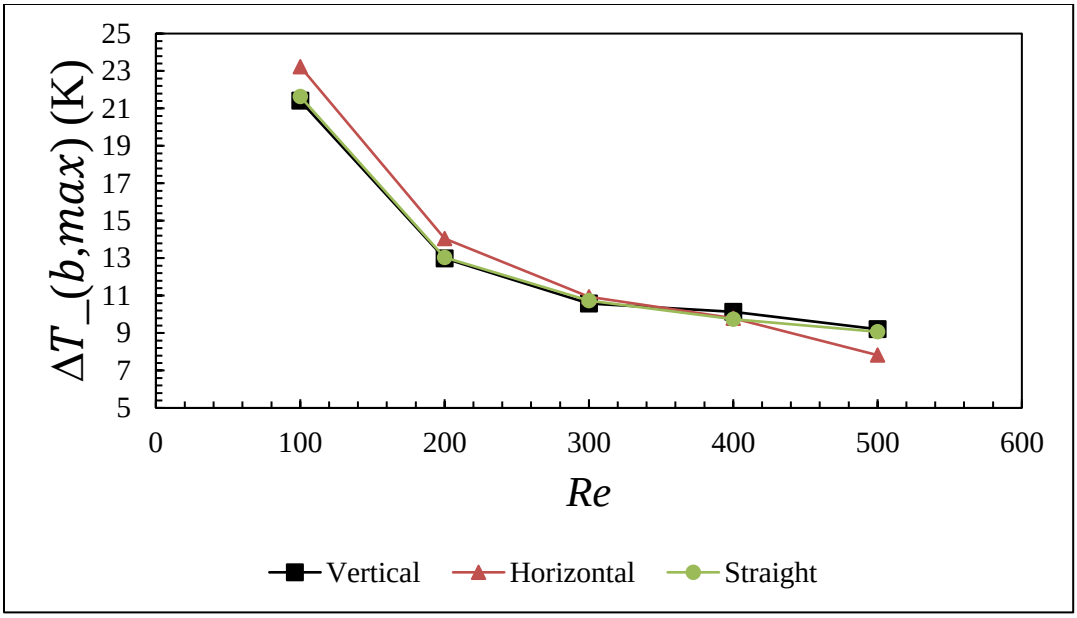

Fig. 23. Maximum temperature difference along the bottom wall of straight, vertical, and horizontal wave MCHS with A = 100 μm and λ = 2000 μm.

vertical wavy designs for Re of 200 and 300 but obtains a lower temperature difference at higher Re. The thermal resistance is shown in Fig. 24 where the straight and vertical wavy design perform very similar for all Re while the horizontal wavy design has a higher thermal resistance up until Re of 400 and then is nearly equal to the straight and vertical wavy design at Re of 500.

3.3 Simulation Results – Constant Amplitude and Changing Wavelength

The rest of the simulations that were conducted had a constant amplitude where A = 100 μm and a changing amplitude varying from $\Delta\lambda = -300$ μm, -150 μm, 150 μm, and 300 μm for both vertical and horizontal wavy designs. These cases were compared to the straight case for all performance metrics. Fig. 25 shows the temperature contours of the bottom wall where the heat flux is applied for the straight case and all horizontal designs with changing wavelengths. It can be seen that the straight channel has the largest temperature difference

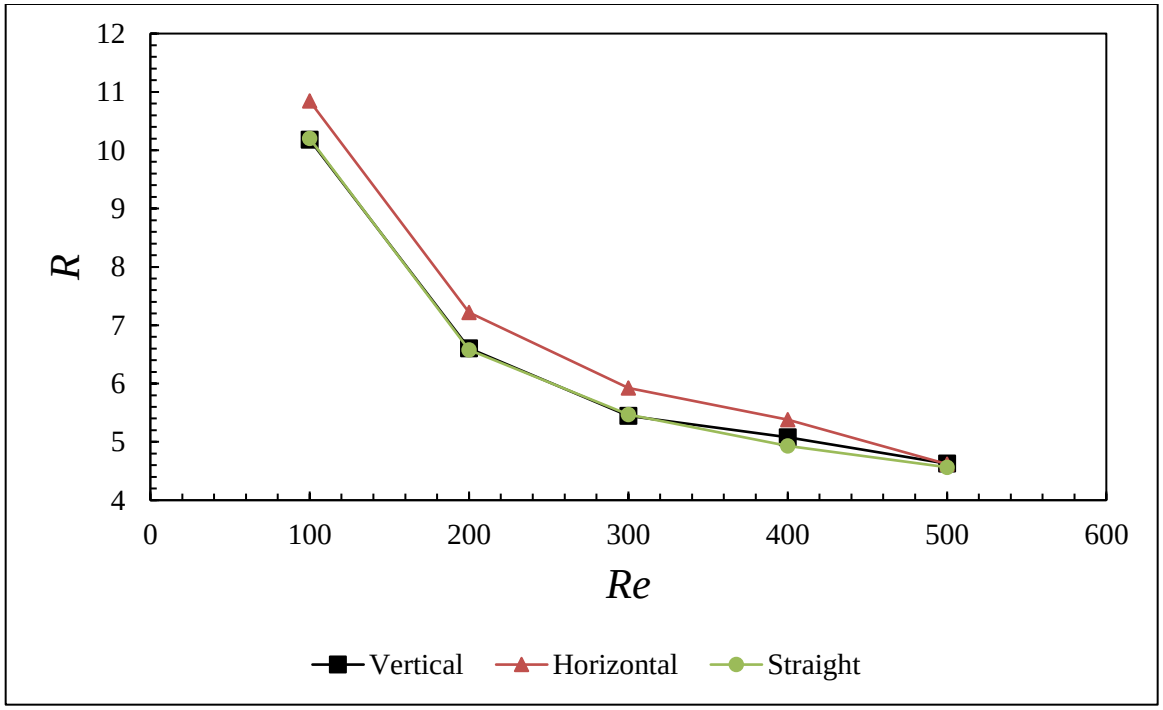

Fig. 24. Thermal resistance of straight, vertical, and horizontal wave MCHS with A = 100 μm and λ = 2000 μm.

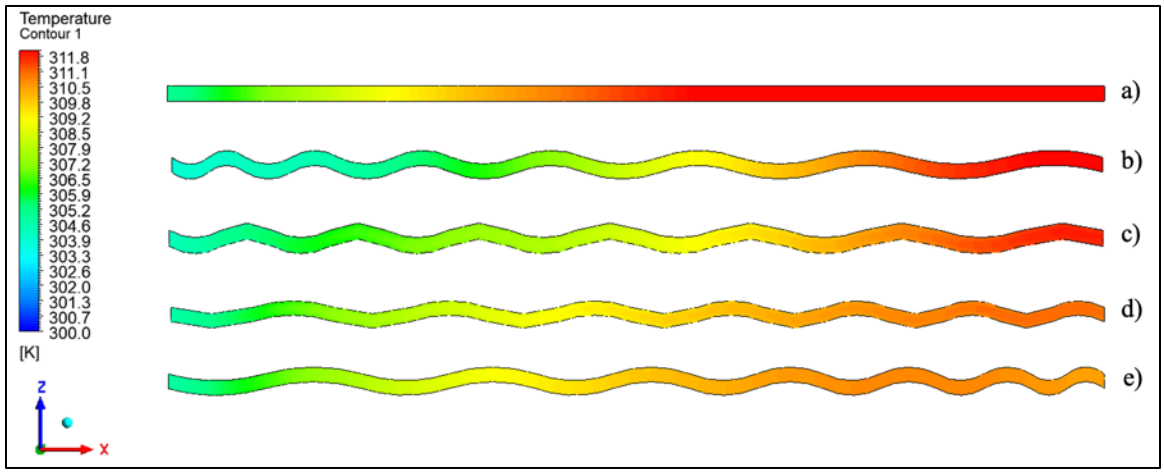

Fig. 25. Temperature contours of bottom wall for (a) straight and horizontal wavy MCHS with (b) $\Delta\lambda = 300$ μm, (c) $\Delta\lambda = 150$ μm, (d) $\Delta\lambda = -150$ μm, (e) $\Delta\lambda = -300$ μm.

along the base and has the worse heat dissipation as the dark red region covers nearly half of the bottom wall. As the change in wavelength decreases, the temperature difference along the bottom wall decreases and better heat dissipation is shown. For the case with $\Delta\lambda = -300\ \mu$m there is no dark red region, but only an orange region that visually displays the hot end of the wall because the heat was more effectively transferred throughout the heat sink for this case.

The Nusselt number is shown in Fig. 26. The horizontal wavy design performed better than the straight and vertical wavy design for all cases of changing wavelengths, with a peak occurring at $\Delta\lambda = 150\ \mu$m. The vertical wavy design only performed better than the straight for cases that had change in wavelength increasing in the flow direction. Fig. 27 shows the maximum temperature difference along the bottom wall which was intuitive for the vertical wavy results because a lower Nu resulted in a higher maximum temperature difference. The horizontal wavy design however, followed a different trend and showed that the lowest maximum temperature difference was found for the case with the largest change in wavelength that decreased in the flow direction. Fig. 28 shows the thermal resistance which showed a very similar trend for both the vertical and horizontal wavy designs. The vertical wavy design with the lowest thermal resistance had a $\Delta\lambda = -150\ \mu$m, while the horizontal wavy design with the lowest thermal resistance had a $\Delta\lambda = -300\ \mu$m.

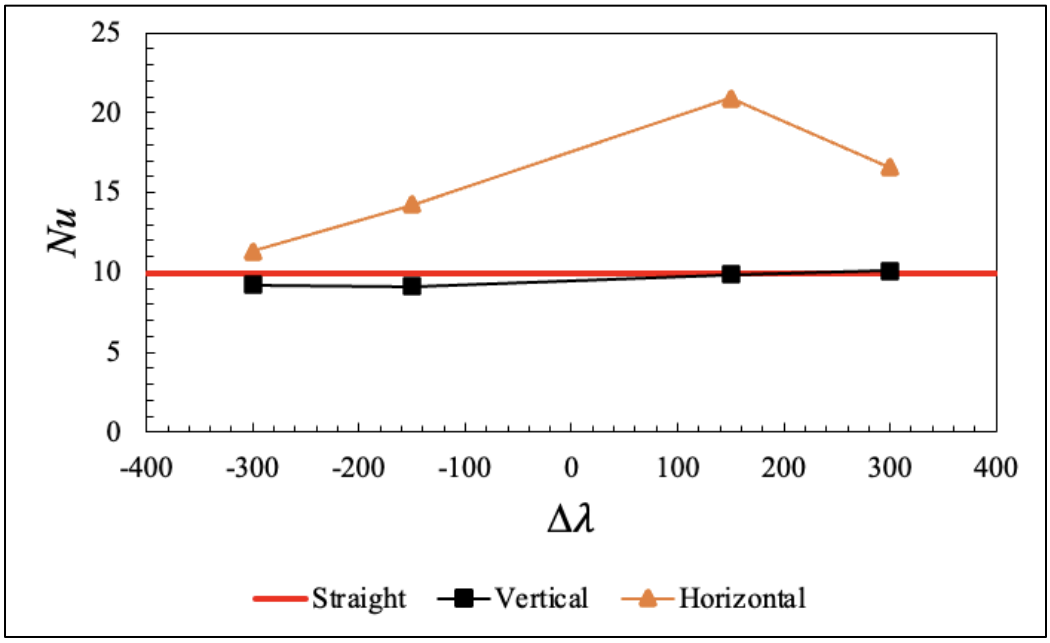

Fig. 26. Nusselt number at Re = 500 as a function of $\Delta\lambda$.

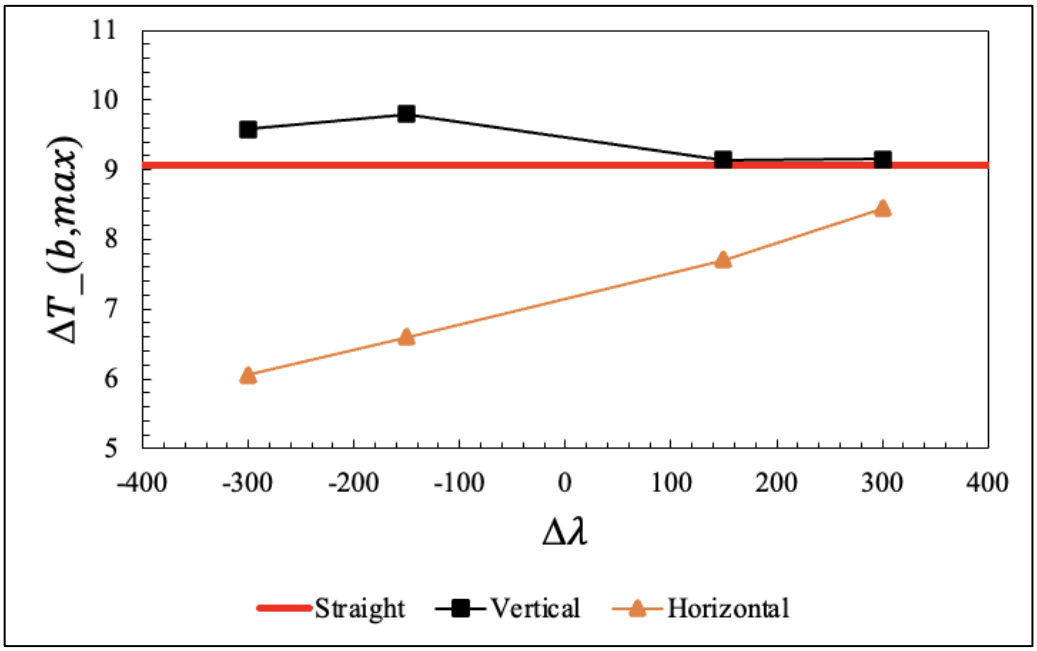

Fig. 27. Maximum temperature difference along the bottom wall at Re = 500 as a function of $\Delta\lambda$.

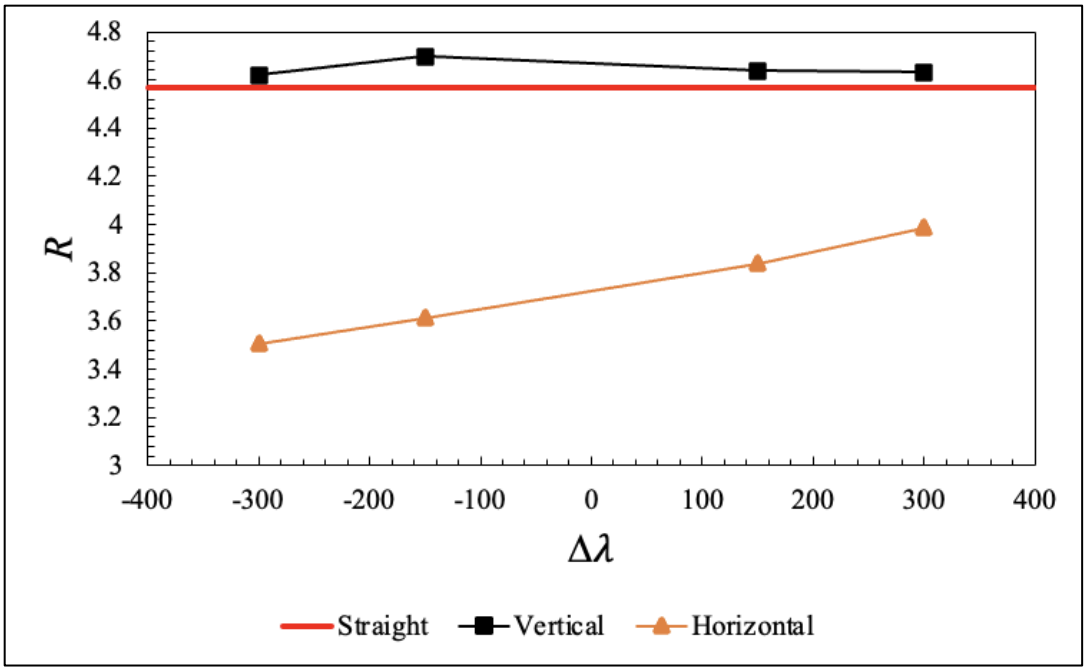

Fig. 28. Thermal resistance at Re = 500 as a function of $\Delta\lambda$.

4 SUMMARY AND CONCLUSION

The results of this study have provided trends that show that the horizontal wavy design performs better than both the straight vertical wavy design for while varying the wavelength. The best performing case for the horizontal design is $\Delta\lambda = -300$ μm that had the largest decrease in wavelength along the flow direction and yielded the lowest thermal resistance and maximum temperature along the base. It can be concluded that the first part of the hypothesis presented in this study is correct, that varying the wavelength along the flow direction will enhance the heat transfer performance for horizontal wavy MCHS. The vertical wavy design on the other hand performed worse than the straight channel obtaining a higher thermal resistance and maximum temperature along the base, and lower Nusselt number which may be due to the high aspect ratio chosen for this study which hindered the growth of the symmetrical vortices produced. These results show that the horizontal wavy design is more effective than the straight and vertical channel especially with larger decrease in wavelength.

There is still more to be investigated regarding horizontal and vertical wavy MCHS to better improve the designs and increase the heat transfer capabilities. One path to pursue is the impact of the channel aspect ratio on heat transfer performance especially for the vertical wavy design because a larger aspect ratio made allow for larger vortices to form within the middle of the channel. Also, it will be interesting to see if varying the amplitude along the flow direction with a constant wavelength will enhance the heat transfer performance for either wavy design. These further investigations may aid in discovering a superior heat sink design.

REFERENCES

[1] D. B. Tuckerman and R. F. W. Pease, "High-performance heat sinking for VLSI," *IEEE Electron Device Lett.*, vol. 2, no. 5, pp. 126-129, 1981.

[2] S. S. Mehendale, A. M. Jacobi, and R. K. Shah, "Fluid flow and heat transfer at micro- and meso-scales with application to heat exchanger design," *Appl. Mech. Rev.*, vol. 53, no. 7, pp. 175-193, 2000.

[3] H. Wang, Z. Chen, and J. Gao, "Influence of geometric parameters on flow and heat transfer performance of micro-channel heat sinks," *Appl. Therm. Eng.*, vol. 107, pp. 870-879, 2016.

[4] P. Gunnasegaran, H. A. Mohammed, and N. H. Shuaib, "The effect of geometrical parameters on heat transfer characteristics of microchannels heat sink with different shapes," *Int. Commun. Heat Mass Transf.*, vol. 37, no. 8, pp. 1078-1086, 2010.

[5] H. M. Metwally and R. M. Manglik, "Enhanced heat transfer due to curvature-induced lateral vortices in laminar flows in sinusoidal corrugated-plate channels," Int. J. Heat Mass Transf., vol. 47, no. 10, pp. 2283-2292, 2004.

[6] R. M. Manglik, J. Zhang, and A. Muley, "Low reynolds number forced convection in three-dimensional wavy-plate-fin compact channels: Fin density effects," Int. J. Heat Mass Transf., vol. 48, no. 8, pp. 1439-1449, 2005.

[7] Y. Sui, P. S. Lee, and C. J. Teo, "An experimental study of flow friction and heat transfer in wavy microchannels with rectangular cross section," Int. J. Therm. Sci., vol. 50, no. 12, pp. 2473-2482, 2011.

[8] H. A. Mohammed, P. Gunnasegaran, and N. H. Shuaib, "Numerical simulation of heat transfer enhancement in wavy microchannel heat sink," *Int. Commun. Heat Mass Transf.*, vol. 38, no. 1, pp. 63-68, 2011.

[9] Y. Sui, C. J. Teo, and P. S. Lee, "Fluid flow and heat transfer in wavy microchannels," *Int. J. Heat Mass Transf.*, vol. 53, no. 13, pp. 2760-2772, 2010.

[10] A. Sakanova, C. C. Keian, and J. Zhao, "Performance improvements of microchannel heat sink using wavy channel and nanofluids," *Int. J. Heat Mass Transf.*, vol. 89, pp. 59-74, 2015.

[11] A. Sakanova, J. Zhao, and K.-J. Tseng, "Investigation on the influence of nanofluids in wavy microchannel heat sink," *IEEE Trans. Compon. Packaging Manuf. Technol.*, vol. 5, no. 7, pp. 956-970, 2015.

[12] J. Zhu, X. Li, and S. Wang, "Performance comparison of wavy microchannel heat sinks with wavy bottom rib and side rib designs," *Int. J. Therm. Sci*., vol. 146, 2019.

[13] L. Lin, J. Zhao, and G. Lu, "Heat transfer enhancement in microchannel heat sink by wavy channel with changing wavelength/amplitude," *Int. J. Therm. Sci*., vol. 118, pp. 423-434, 2017.

[14] B. Dang, M. S. Bakir, and D. C. Sekar, "Integrated microfluidic cooling and interconnects for 2D and 3D chips," *IEEE Trans. Adv. Packaging*, vol. 33, no. 1, pp. 79-87, 2010.

[15] C. Nadjahi, H. Louahlia, and S. Lemasson, "A review of thermal management and innovative cooling strategies for data center," *Sustain. Comput.: Inform. Syst*., vol. 19, pp. 14-28, 2018.

[16] F. M. White, *Fluid Mechanics*. New York, NY, USA: McGraw Hill, 2011.

[17] ANSYS, " Lecture 9: Best practice guidelines: Introduction to ANSYS fluent," ANSYS, Inc. April 2016. https://www.kth.se/social/files/57149285f27654646b25d53b/05-Quality-ANSYS.pdf.

[18] P. Lee, S. V. Garimella, and D. Liu, "Investigation of heat transfer in rectangular microchannels," *Int. J. Heat Mass Transf*., vol. 48, no. 9, pp. 1688-1704, 2005.

[19] G. Xie, J. Liu, and Y. Liu, "Comparative study of thermal performance of longitudinal and transversal-wavy microchannel heat sinks for electronic cooling," *J. Electron. Packaging*, vol. 135, no. 2, 2013.

[20] F. P. Incropera, *Fundamentals of Heat and Mass Transfer*. New York, NY, USA: Wiley, 1985.